AGU PUBLICATIONS

Geophysical Research Letters

RESEARCH LETTER
10.1002/2016GL071899

Key Points:
- Amplitude of subseasonal SST variability over the Seychelles-Chagos Thermocline Ridge (SCTR) is highly correlated with ENSO
- During El Niño, SST is warmer and mixed layer is deeper than normal over the SCTR
- The deeper mixed layers with warmer upper ocean conditions reduce the subseasonal SSTA variability over the SCTR

Supporting Information:
- Supporting Information S1
- Figure S1
- Figure S2
- Figure S3
- Figure S4
- Figure S5
- Figure S6
- Figure S7

Correspondence to:
E. Jung,
eunsil.jung@gmail.com

Citation:
Jung, E., and B. P. Kirtman (2016), ENSO modulation of tropical Indian Ocean subseasonal variability, *Geophys. Res. Lett.*, *43*, 12,634–12,642, doi:10.1002/2016GL071899.

Received 7 MAY 2016
Accepted 16 NOV 2016
Accepted article online 17 NOV 2016
Published online 30 DEC 2016

ENSO modulation of tropical Indian Ocean subseasonal variability

Eunsil Jung[1,2] and Ben P. Kirtman[1]

[1]Rosenstiel School of Marine and Atmospheric Science, University of Miami, Miami, Florida, USA, [2]Now at National Institute of Meteorological Sciences, Jeju, South Korea

Abstract In this study, we use 30 years of retrospective climate model forecasts and observational estimates to show that El Niño/Southern Oscillation (ENSO) affects the amplitude of subseasonal variability of sea surface temperature (SST) in the southwest Indian Ocean, an important Tropical Intraseasonal Oscillation (TISO) onset region. The analysis shows that deeper background mixed-layer depths and warmer upper ocean conditions during El Niño reduce the amplitude of the subseasonal SST variability over Seychelles-Chagos Thermocline Ridge (SCTR), which may reduce SST-wind coupling and the amplitude of TISO variability. The opposite holds for La Niña where the shallower mixed-layer depth enhances SST variability over SCTR, which may increase SST-wind coupling and the amplitude of TISO variability.

1. Introduction

Subseasonally varying sea surface temperature (SST) and precipitation explains 20–30% of the total variability of SST and precipitation over the Indo-western Pacific (Figures 1a and 1b), suggesting that variability on subseasonal (30–90 days) time scales plays an important role in the tropical Indian Ocean. Subseasonally varying deep convection over the Indo-Pacific is one of the most organized large-scale perturbations in the tropics. This so-called Tropical Intraseasonal Oscillation (TISO) initiates over the Indian Ocean, propagates into the Pacific, and impacts many global weather and climate phenomena, such as El Niño/Southern Oscillation (ENSO), extreme weather in the Northern Hemisphere, Asian and Australian monsoons, and tropical cyclone activity among many other impacts [*Zhang*, 2013, and references therein]. However, the individual TISO events are not well predicted beyond 2–4 weeks with most current prediction systems [*Waliser et al*., 2003; *Hung et al*., 2013; *Klingaman et al*., 2015]. In the Pacific, on the other hand, interannual and longer periods are the dominant time scales of variability (Figures 1a and 1b). ENSO, for example, occurs in the central to eastern Pacific on interannual (2–7 years) time scales with significant global socio-economic and environmental impacts and has a predictability of about 6–9 months before its mature stage [e.g., *Kirtman and Schopf*, 1998; *Collins et al*., 2002].

There have been many studies to determine whether and how these two dominant modes interact with each other. Previous studies show that a boreal winter TISO, which is commonly referred to as the Madden-Julian Oscillation (MJO) [*Madden and Julian*, 1972], interacts and affects ENSO through westerly wind bursts. Anomalously strong westerly winds associated with the passage of the MJO in the western Pacific modify thermocline structures in the equatorial Pacific Ocean and, in turn, play a role in triggering ENSO events [e.g., *Weickmann*, 1991; *Kessler et al*., 1995; *McPhaden*, 1999; *Kessler and Kleeman*, 2000; *Lopez and Kirtman*, 2013]. ENSO modulations of the MJO have been also studied [e.g., *Pohl and Matthews*, 2007; *Fink and Speth*, 1997; *Tam and Lau*, 2005]. For example, MJO activity extends farther east than usual [e.g., *Woolnough et al*., 2000; *Tam and Lau*, 2005], and the lifetime is shorter than usual during El Niño conditions [*Pohl and Matthews*, 2007; *Tam and Lau*, 2005]. It has been also suggested that changes in MJO associated with ENSO, in turn, affect the evolution of ENSO [e.g., *Kug et al*., 2008]. However, to date, no significant simultaneous correlations have been found between the amplitude of MJO activity over the Indian Ocean and the state of ENSO [e.g., *Slingo et al*., 1999; *Hendon et al*., 1999].

TISO is fundamentally an atmospheric phenomenon. However, observational and modeling studies over the past decades suggest that TISO is affected by the atmosphere-ocean coupled processes [*DeMott et al*., 2015, and references therein], although its existence may not be inherently coupled [e.g., *Sobel and Maloney*, 2013]. Motivated by the nature of the TISO being a coupled system [e.g., *Waliser et al*., 1999; *Webster et al*., 1999], the current study examines the amplitude of subseasonal SST variability over the southwestern Indian Ocean and

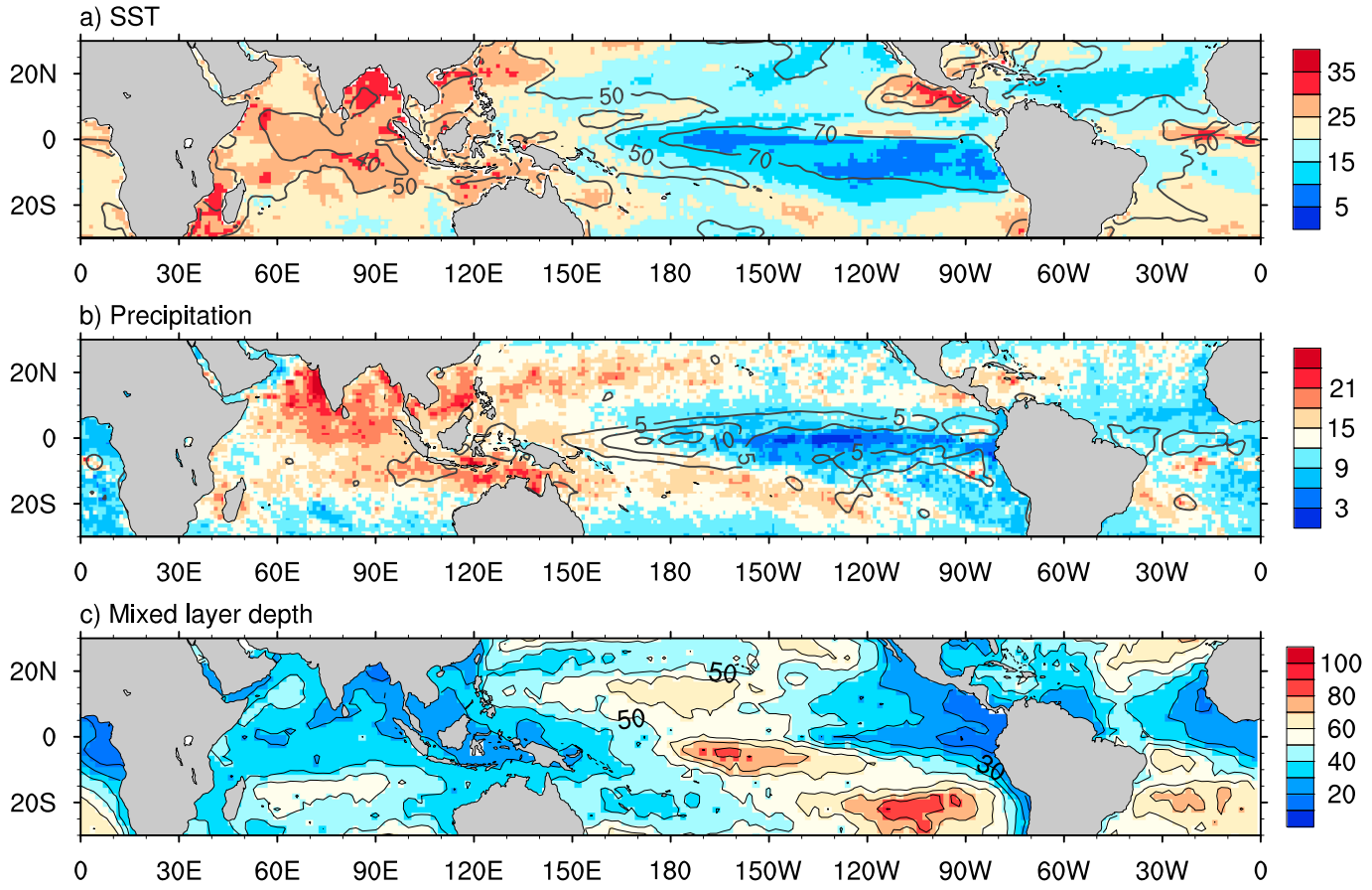

Figure 1. (a and b) Percentage of subseasonal (shading) and interannual (contour) variability of (a) SST and (b) precipitation anomalies over Indo-Pacific for all seasons of 1982–2014 (Figure 1a) and 1982–2012 (Figure 1b). (c) Climatology of mixed-layer depth (MLD) (m) for 1961–2008.

its connection to ENSO. This regional focus on the southwest Indian Ocean is because of its importance in the initiation of TISO. We compare the analysis of observational data with retrospective climate model forecasts to assess the potential predictability of TISO modulations by ENSO. Throughout the text, TISO and MJO are used interchangeably, and the terminology of subseasonal is used to encompass all variability on this time scale.

2. Data and Method

2.1. Model Description

The model used for this study is the National Center for Atmospheric Research Community Climate System Model version 4.0 (CCSM4.0) [see *Neale et al.*, 2010]. The performance of the model based on a full set of metrics is described in a *Journal of Climate* special collection [e.g., *Gent et al.*, 2011], and the model's skill in simulating and predicting tropical Indo-Pacific variability is described in *Meehl et al.* [2012]. The model is currently used as routine real-time predictions as part of North American Multimodel Ensemble [*Kirtman et al.*, 2014]. The 10 ensemble members of CCSM4 forecasts are initialized at the first day of each month over the period 1982–2009. We showed the results from the January-initialized forecasts that were initialized on every 1 January 1982–2009 using the observational estimates. Each forecast is for lead times up to 1 year.

2.2. Observational Estimates

The observational data used in this study are NOAA Advanced Very High-Resolution Radiometer Global Blended SST (level 4 [*Reynolds et al.*, 2007], ftp://ftp.nodc.noaa.gov/pub/data.nodc/ghrsst/L4/GLOB/NCDC/AVHRR_OI), Tropical Rainfall Measuring Mission precipitation (3B42 v7 [*Huffman et al.*, 2007], ftp://disc2.nascom.nasa.gov/ftp/data/s4pa//TRMM_L3/TRMM_3B42_daily/), flux data from the Woods Hole Oceanographic

Institution (http://oaflux.whoi.edu/) [*Yu et al*., 2008], mixed-layer depth (MLD) from French Research Institute for Exploration of the Sea (Ifremer, http://www.ifremer.fr/) [*de Boyer Montégut et al*., 2004, 2007], and sea surface heights (SSHs) from Archiving, Validation, and Interpretation of Satellite Oceanographic data (http://www.aviso.altimetry.fr/en/data.html). Daily data (except the MLD) with spatial resolutions of $0.25° \times 0.25°$ (except for 1° of flux) are interpolated to model grids ($1° \times 1°$) and used for 1982–2009 unless otherwise stated. SSH is used as a proxy of thermocline depth. More detailed information of observational data is given in the supporting information.

2.3. Method

Daily anomalies are computed by subtracting the climatological annual cycle from the daily means. This daily anomaly is referred to as all time scales in this study. Subseasonal time scale refers to daily anomaly that is Lanczos band-pass filtered in the period of 20–100 days with 201 weights. Monthly anomalies are computed by subtracting the climatological annual cycle from the monthly means. Interannual time scales refer to daily or monthly anomalies that are low-pass filtered with cutoff period of 120 days. To isolate how the amplitude of subseasonal SST anomaly (SSTA) variability relates to ENSO, we first square the daily SSTA. Then a running average of *N* days (e.g., 30 and 90 days) is performed, and lastly, the annual cycle of the running averaged-squared SSTA is removed. We refer this final field as the low-frequency-amplitude modulation (LFAM) of the subseasonal SST variability.

3. Results and Discussion

The ocean and atmosphere interact by exchanging heat, fresh water, and momentum at the air-sea interface. On average, the ocean mixed layer is the upper 50 m of the ocean in the tropics (43 ± 7 m from *de Boyer Montégut et al*. [2007]), where the immediate effects of atmosphere-ocean coupling are felt. Over the Indo-western Pacific Ocean, the strong subseasonal SST and precipitation variability occur in the shallow mixed-layer regions (Figure 1c), suggesting a close relationship between the coupled process (e.g., TISO) and MLD. Indeed, the strength and phase speed of TISO varied with MLD in slab ocean model experiments [e.g., *Maloney and Sobel*, 2004]. Further, a shallower MLD was observed before the onset of MJO, and then the ML became deeper as the convection became active [*Drushka et al*., 2012; *Chi et al*., 2014; *Duvel et al*., 2004].

Over the Indian Ocean, prominent subseasonal SST variability is found in the southwestern Indian Ocean along the band of 5–15°S including a Seychelles-Chagos Thermocline Ridge (SCTR) [e.g., *Vialard et al*., 2009; *Jayakumar et al*., 2011] (Figure S2 in the supporting information). The SCTR corresponds to a region where the thermocline is close to the surface, resulting in a shallow mixed layer. This year-round feature is more pronounced in boreal winter and spring (Figure S1), contributing to strong air-sea interactions [e.g., *Duvel et al*., 2004; *Vialard et al*., 2009; *Jayakumar et al*., 2011; *Xie et al*., 2002]. Accordingly, more frequent TISO events are observed in the SCTR during boreal winter and spring, although they do occur throughout the year [*Jones et al*., 2004; *Madden and Julian*, 1994]. Since it has been suggested that the coupled processes in the SCTR region affect TISO variability [e.g., *Duvel et al*., 2004; *Vialard et al*., 2009; *Jayakumar et al*., 2011; *Xie et al*., 2002; *DeMott et al*., 2015], and further, forecasts capture the SST variability fairly well in that region (Figure S2), we focus our analysis on this area of the Indian Ocean hereafter.

The subseasonal SST variability over the SCTR is examined in Figures 2a and 2b by calculating correlations between SCTR index and all time scale SSTA over the tropical Ocean. We define the SCTR index as the area-averaged subseasonal SSTA in the area of 5°S–10°S, 50–80°E. In Figures 2a and 2b, both forecasts and observational estimates show that subseasonal SSTA variability in the SCTR is highly correlated with all time scale SSTA exclusively over the Indian Ocean with localized maximum in the SCTR. In contrast, there is little correlation with any other regions over the tropics.

To diagnose whether there is some low-frequency modulation of subseasonal variability that can be teleconnected and predicted beyond the Indian Ocean, we introduce an index that measures the modulation of the low-frequency amplitude of subseasonal variability in the SCTR (see section 2.3) and then relate this index to interannually varying SSTA in the tropical ocean (Figures 2c–2f). Compared with Figures 2a and 2b, the LFAM of subseasonal SSTA shows an enhanced correlation to the Pacific SSTA (correlation ≥ 0.25), particularly for longer running averages. This indicates that the LFAM of subseasonal SSTA variability in the SCTR region is

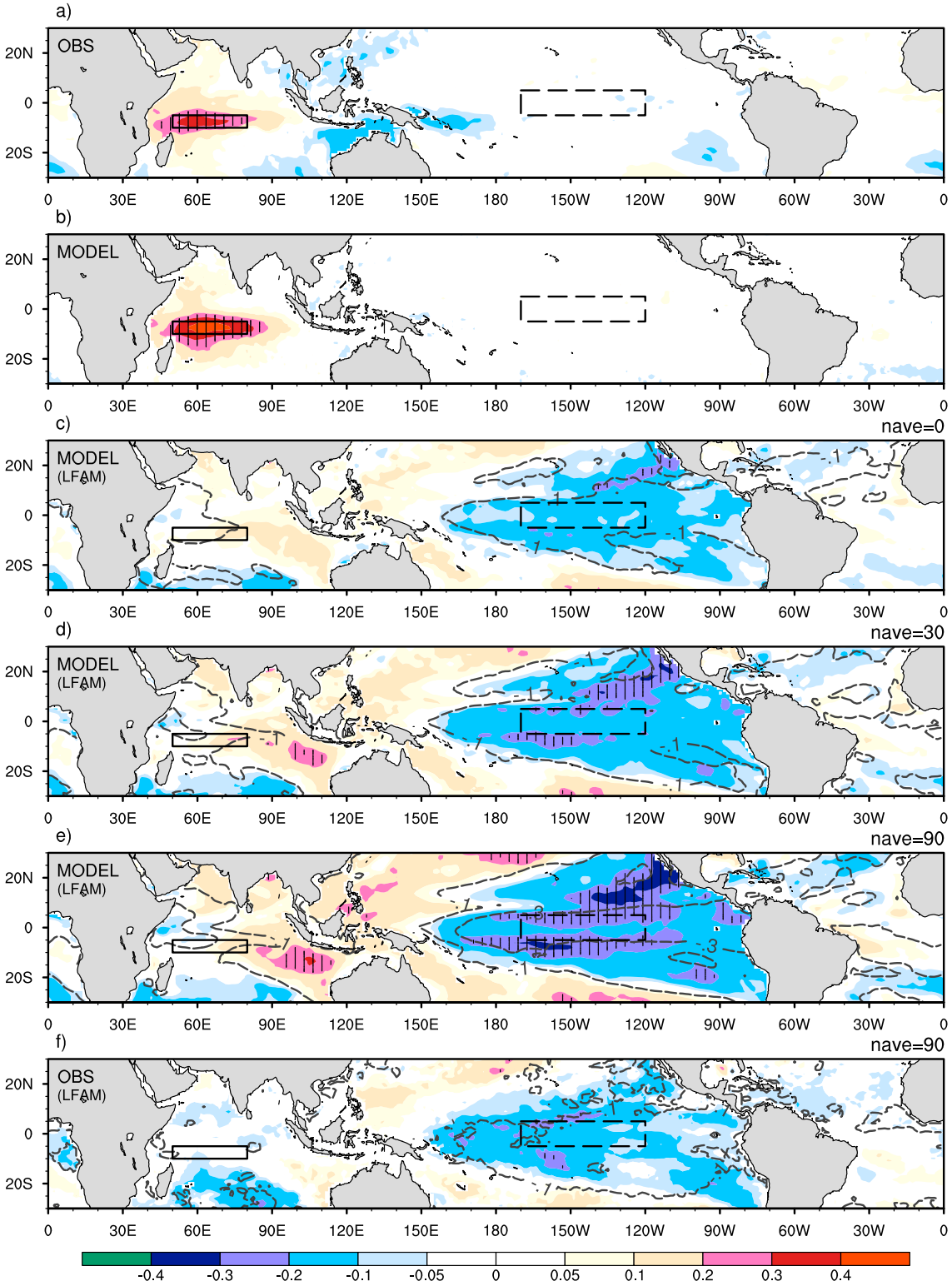

Figure 2. The impacts of SCTR subseasonal SST variability on the Indo-Pacific SST are shown as (a and b) correlations between subseasonal SCTR index (area-averaged SSTA in the SCTR region) and all time scale Indo-Pacific SSTA from observational estimates (Figure 2a) and forecasts (Figure 2b), and as (c–f) correlations between subseasonal SCTR low-frequency-amplitude modulation (LFAM) index and interannual Indo-Pacific SSTA from forecasts (Figures 2c–2e) and observational (Figure 2f) estimates. Running averages of 0 (nave = 0) (Figure 2c), 30 (nave = 30) (Figure 2d), and 90 days (nave = 90) (Figures 2e and 2f) are used. The hashed area is statistically significant at the 90% confidence level. Correlations between LFAM-SCTR easterly wind stress (τ_x) and interannual Indo-Pacific SSTA are shown as dashed contours in Figures 2c–2f. Contour intervals of 0.1 and 0.3 are shown. Niño 3.4 and SCTR regions are shown as boxes.

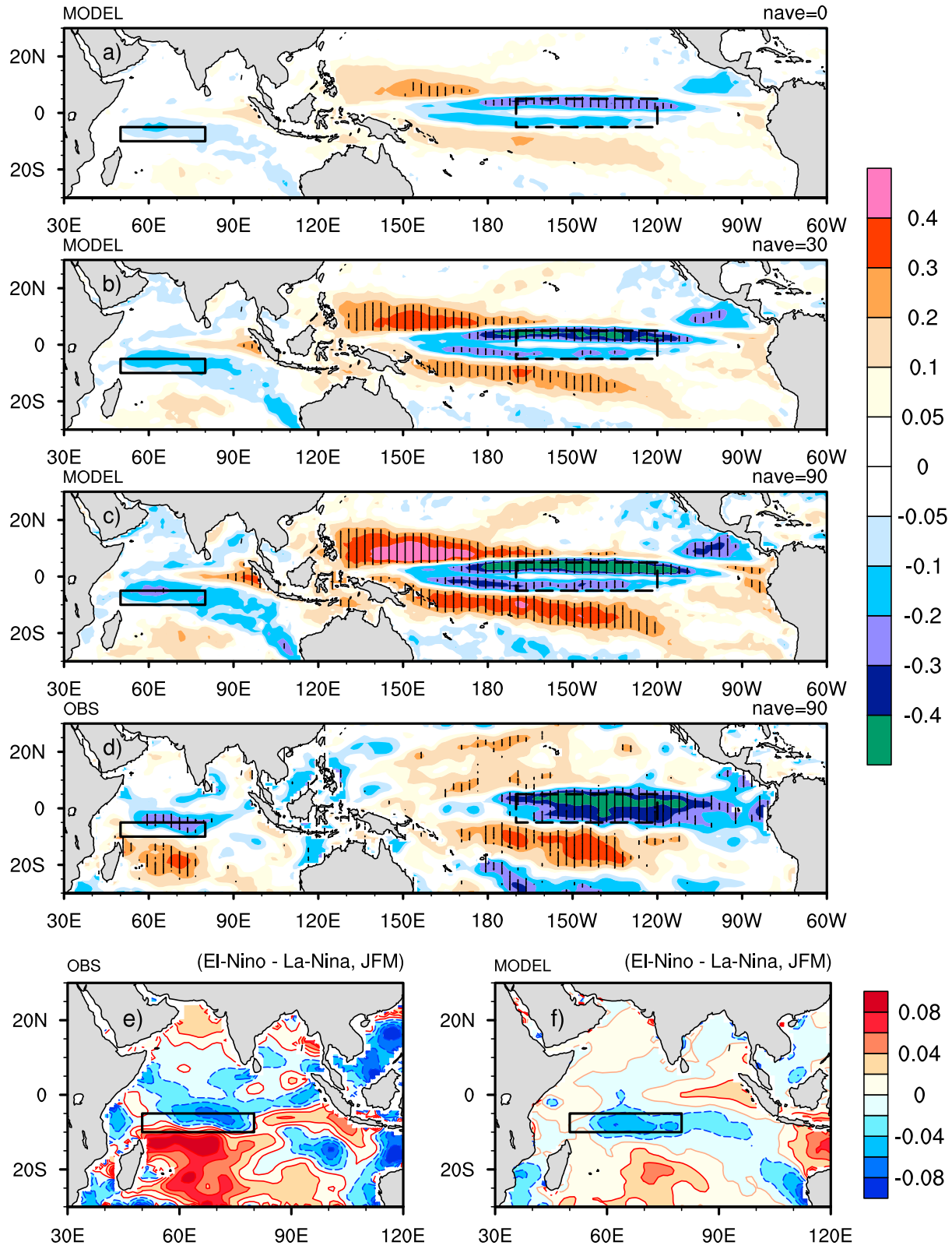

Figure 3. The impact of ENSO on the subseasonal SST variability shown as (a–d) correlations between interannual Niño 3.4 SST index and LFAM of subseasonal SSTA in the Indo-Pacific for all seasons of 1982–2009, from forecasts (Figures 3a–3c) and observational (Figure 3d) estimates. Running averages of 0, 30, and 90 days (nave = 90) are shown. The hashed area is significant at the 90% confidence level. (e and f) The variance of subseasonal SSTA difference between JFM El Niño and JFM La Niña for the years of 1982–2009 from observational estimates (Figure 3e) and forecasts (Figure 3f). Niño 3.4 and SCTR regions are shown as boxes.

related to the interannual Pacific SSTA variability (e.g., ENSO). The same correlation pattern is shown from observational estimates (Figure 2f) using a running average of 90 days. Although the correlation is somewhat weaker, the teleconnection to the Pacific is readily apparent. Essentially, Figure 2 suggests that there is potential to predict the mean seasonal *amplitude* of subseasonal SSTA variability in the southwestern Indian Ocean due to Pacific seasonal-to-interannual SSTA variations.

The similar analysis as Figure 2 was made for the zonal winds (contours in Figure 2), surface heat flux (not shown), SSH, mixed-layer, and thermocline depths (Figure S3). Among them, the SCTR-LFAM of easterly wind stress (τ_x) and MLD anomalies showed the same ENSO-like pattern as in Figure 2, suggesting that the amplitudes of subseasonal winds and MLD over the SCTR vary with ENSO phase. Given that, during El Niño, temperature gradient across the mixed layer would be of great importance as the amplitude of MLD variability enhances. In contrast, there was little correlation between Niño 3.4 SST and LFAM of surface heat flux (not shown), thermocline depth, and SSH over the SCTR (Figure S3).

The reversed analysis is made in Figure 3 to confirm the relationships between the state of ENSO and SCTR-LFAM of SSTA shown in Figure 2. Figure 3 shows correlations between Indo-Pacific LFAM of SSTA at all grid points at subseasonal time scales and ENSO index at interannual time scales. The ENSO index is an area-averaged SSTA in the Niño 3.4 region (120°W–170°W, 5°S–5°N). In Figure 3, ENSO and subseasonal SSTA amplitude are significantly and negatively correlated near the SCTR (consistent with Figure 2, confirming that the SCTR-LFAM of SSTA is correlated with the state of ENSO) and along the central to eastern equatorial Pacific, showing stronger correlations in the observational estimates. In contrast, ENSO and subseasonal SSTA amplitude are positively and significantly correlated south to SCTR and near central Pacific (150°E–120°W) off the equator, although the positive correlations over the northwestern Pacific (south to SCTR) are overestimated (underestimated) in the forecasts. The results are consistent with earlier observational works [e.g., *Gutzler*, 1989; *Tam and Lau*, 2005] that showed an enhanced subseasonal activity of low-level zonal winds near and east of the dateline, and weaker variance over the western Pacific during El Niño. However, no significant simultaneous correlations were found by these authors over the Indian Ocean. The SSTA variance difference between El Niño and La Niña years (Figures 3e and 3f) also shows that subseasonal SSTA variance near SCTR is substantially reduced during January-February-March (JFM) El Niño years, whereas it is greatly enhanced during La Niña years. The year of El Niño (La Niña) in Figures 3e and 3f is defined as a year in which the SSTA that is averaged for 3 months is larger than positive (negative) 0.5°C for three consecutive months. Further, the state of ENSO is highly correlated with the LFAM of MLD near SCTR but not thermocline depth (Figure S4), which is consistent with Figure S3.

Changes in the mean state of the atmosphere and ocean that is associated with ENSO are examined in Figure 4 as correlations between ENSO index and Indo-Pacific SST, MLD, and thermocline depth anomalies on interannual time scales. During El Niño, SST over the Indian Ocean is warmer than normal overall (Figures 4a and 4b), and easterly anomalies prevail in the SCTR (not shown). Furthermore, El Niño is correlated with deeper MLD and thermocline depths in the SCTR (Figures 4c–4f). The variability of interannual thermocline depth in this region is also known to be associated with the Indian Ocean Dipole (IOD) [*Saji et al*., 1999], which IOD tends to occur with ENSO (e.g., +IOD in Figures 4a and 4b), but can happen without ENSO [e.g., *Fischer et al*., 2005]. Changes in MLDs are of importance for air-sea coupled processes, such as those associated with TISO, since the mixed layer is the interface where the ocean and atmosphere interacts and is highly correlated with the subseasonal variability of SST and precipitation [e.g., *Maloney and Sobel*, 2004; *Drushka et al*., 2012; *Chi et al*., 2014; *Duvel et al*., 2004; *Jayakumar et al*., 2011; *Xie et al*., 2002; *Matthews et al*., 2014; *Moum et al*., 2014] (see also Figure 1). The impact of interannual MLD modulation on the LFAM of SST and wind stress variability is shown in Figure S5. The correlations between two show that deeper mixed-layer anomalies are correlated with reduced SSTA amplitude in the Indian Ocean, in particular along the 5–10°S (Figures S5a and S5ab), and reduced westerly anomalies over the Indian Ocean (Figures S5c and S5d), which is not favorable for the initiation of TISO.

Over the SCTR, changes in MLD are closely related to changes in SSTA at subseasonal time scales [*Halkides et al*., 2015, and references therein]. In general, when winds become stronger, the mixed layer becomes deeper and colder because stronger winds (and weaker solar radiation) make the mixed layer more turbulent via mechanical mixing (and by decreasing stratification), which entrains relatively colder water from below the mixed layer. However, during El Niño, in addition to the deeper ML that has a larger inertia, the upper

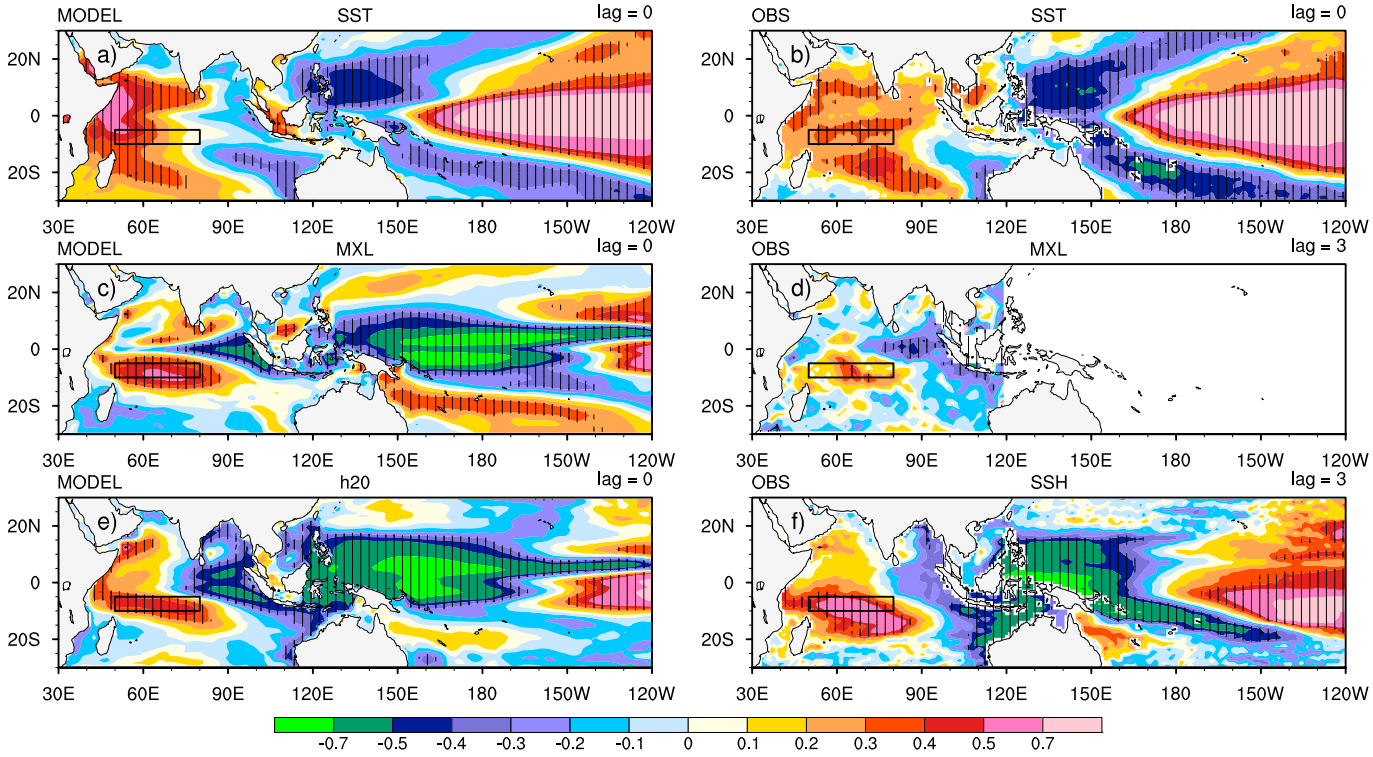

Figure 4. Correlations between interannual oceanic variability and ENSO. Correlations are calculated between Niño 3.4 SST index and (a and b) SST, (c and d) MLD, and (e and f) thermocline depth anomalies in the forecast (Figures 4a, 4c, and 4e) and observational (Figures 4b, 4d, and 4f) estimates on interannual time scales. Correlations at lag 0 and 3 months where the maximum correlations are found in the mixed-layer and thermocline depths are shown in Figures 4c–4f. SSH anomaly is used for the thermocline depth (h20) in Figure 4f. SCTR is shown as a box. The hashed area is significant at the 90% confidence level.

ocean is warmer than usual in the SCTR (Figures 4 and S6). Therefore, the water that entrains into the ML is a similar temperature as the ML, which also results in smaller SSTA variability. Since the amplitude of MLD variability enhances during El Niño (Figures S3a–S3c), the similar ocean temperature right below the ML in the SCTR plays a role in reducing the subseasonal SSTA variability.

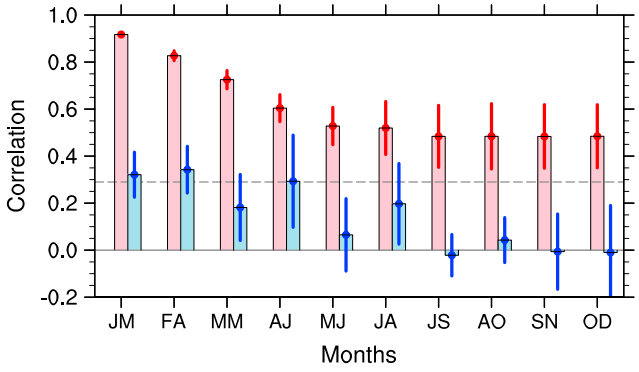

Figure 5. Prediction skill of LFAM-SSTA in the SCTR (blue) and Niño 3.4 index (red) from January-initialized forecasts. Prediction skill is calculated from correlations between predicted and observed SSTA with monthly data of 1982–2014. Mean $\pm$ 1σ is shown as a vertical bar. The LFAM-SSTA is calculated with the 3 month mean of SSTA without running averages (blue). The initials of the first and last months are shown on the *x* axis (e.g., "JM" indicates January–March). Correlations above the dotted line are significant at the 90% confidence level.

Although ENSO is highly correlated with interannual thermocline variations in the SCTR (Figures 4e and 4f), it should also be noted that there is no LFAM of subseasonal thermocline depth that is associated with ENSO (Figures S3 and S4), indicating that the role of ENSO in TISO is linked via the MLD modulation, not the thermocline depth feedback. This is because the thermocline requires longer time to adjust to wind forcing compared to the mixed layer depth. Deeper mixed layers associated with stronger winds over the SCTR are well captured in the forecasts (Figure S7a). The predicted total net surface heat fluxes also agree with observed fluxes in the SCTR region (Figures S7b–S7e). The analyses in this study are made with a year-

round data set, yet the results are robust regardless of seasons (not shown), but the correlations are stronger for boreal winter months (e.g., JFM) because both the subseasonal SSTA variability over SCTR and ENSO are the most active during boreal winter.

The prediction skill of SCTR-LFAM is assessed by calculating correlations between predicted and observed LFAM-SCTR index (Figure 5). The amplitude of SSTA is calculated by the same method as LFAM using seasonal mean SSTA. Correlations between predicted and observed ENSO index are also shown in Figure 5 to show the model performance relative to ENSO prediction. In Figure 5, Niño 3.4 SST has about 6–8 months of prediction skill in the forecasts assuming a threshold of 0.5. However, predicting the amplitude of subseasonal variability is more challenging. Correlations are about 0.32 until April then gradually drop with substantial fluctuations. In Figure 5, ENSO explains about 7% of LFAM subseasonal SCTR-SSTA variability until about April.

4. Summary and Conclusion

This study examines the interactions between ENSO and the amplitude of subseasoanal SST variability over the SCTR, a dominant TISO onset region. We use climate model forecasts to facilitate the direct comparisons with observational estimates for 1982–2009. The analysis shows that the low-frequency amplitude of subseasonal SST variability is correlated with ENSO. During El Niño, the background mixed-layer and thermocline depths are deeper than normal. The deeper mixed layers with warmer upper ocean conditions, modulated by El Niño, in turn, play a role in reducing the amplitude of subseasonal SSTA variability over SCTR, which possibly reduces SST-wind coupling and the amplitude of TISO variability via air-sea coupled process [e.g., *Webster et al*., 1999; *DeMott et al*., 2015, and references therein]. The opposite holds for La Niña where the shallower mixed-layer depth enhances SST variability over SCTR, which may increase SST-wind coupling and the amplitude of TISO variability.

This study highlights that ENSO modulates the low-frequency amplitude of subseasonal SST variability over SCTR through the MLD modulation, suggesting that ENSO can be used to predict the mean seasonal *amplitude* of subseasonal variability over the Indian Ocean. Recently, *Benedict et al*. [2015] also showed that the MJO propagation was influenced by the Pacific SSTA rather than the local Indian Ocean SSTA. Changes in TISO associated with ENSO, in turn, affect the evolution of ENSO [*Kug et al*., 2008], and thus, it is also possible that the enhanced subseasonal variability over the Indian Ocean during La Niña makes the evolution of La Niña less predictable.

Acknowledgments
The model data set for this paper is available at http://www.cpc.ncep.noaa.gov/products/NMME/. The observational estimate data set is available through anonymous ftp given in section 2 for details. The research was supported by NOAA grants NA10OAR4320143, NA14OAR4830127, and NA12OAR4310089 and ONR grant N000141310844. We thank two anonymous reviewers for their constructive and comprehensive comments on the manuscript.

References

Benedict, J. J., M. S. Pritchard, and W. D. Collins (2015), Sensitivity of MJO propagation to a robust positive Indian Ocean dipole event in the superparameterized CAM, *J. Adv. Model. Earth Syst.*, *7*, 1901–1917, doi:10.1002/2015MS000530.

Chi, N.-H., R.-C. Lien, E. A. D'Asaro, and B. B. Ma (2014), The surface mixed layer heat budget from mooring observations in the central Indian Ocean during Madden-Julian Oscillation events, *J. Geophys. Res. Oceans*, *119*, 4638–4652, doi:10.1002/2014JC010192.

Collins, M., D. Frame, B. Sinha, and C. Wilson (2002), How far ahead could we predict El Niño?, *Geophys. Res. Lett.*, *29*(10), 1492, doi:10.1029/2001GL013919.

de Boyer Montégut, C., G. Madec, A. S. Fischer, A. Lazar, and D. Iudicone (2004), Mixed layer depth over the global ocean: An examination of profile data and a profile-based climatology, *J. Geophys. Res.*, *109*, C12003, doi:10.1029/2004JC002378.

de Boyer Montégut, C., J. Mignot, A. Lazar, and S. Cravatte (2007), Control of salinity on the mixed layer depth in the world ocean: 1. General description, *J. Geophys. Res.*, *112*, C06011, doi:10.1029/2006JC003953.

DeMott, C. A., N. P. Klingaman, and S. J. Woolnough (2015), Atmosphere-ocean coupled processes in the Madden-Julian Oscillation, *Rev. Geophys.*, *53*, 1099–1154, doi:10.1002/2014RG000478.

Drushka, K., J. Sprintall, S. T. Gille, and S. Wijffels (2012), In situ observations of Madden-Julian Oscillation mixed layer dynamics in the Indian and western Pacific Oceans, *J. Clim.*, *25*, 2306–2328.

Duvel, J. P., R. Roca, and J. Vialard (2004), Ocean mixed layer temperature variations induced by intraseasonal convective perturbations over the Indian Ocean, *J. Atmos. Sci.*, *61*, 1004–1023, doi:10.1175/1520-0469(2004)061<1004:OMLTVI>2.0.CO;2.

Fink, A., and P. Speth (1997), Some potential forcing mechanisms of the year-to-year variability of the tropical convection and its intraseasonal (25–70 day) variability, *Int. J. Climatol.*, *17*, 1513–1534.

Fischer, A. S., P. Terray, E. Guilyardi, S. Gualdi, and P. Delecluse (2005), Two independent triggers for the Indian ocean dipole/zonal mode in a coupled GCM, *J. Clim.*, *18*(17), 3428–3449.

Gent, P. R., et al. (2011), The Community Climate System Model Version 4, *J. Clim.*, *24*, 4973–4991, doi:10.1175/2011JCLI4083.1.

Gutzler, D. S. (1989), Interannual fluctuations of intraseasonal variance of near-equatorial zonal winds, *J. Geophys. Res.*, *96*, 3173–3185, doi:10.1029/90JD01831.

Halkides, D. J., D. E. Waliser, T. Lee, D. Menemenlis, and B. Guan (2015), Quantifying the processing controlling intraseasonal mixed-layer temperature variability in the tropical Indian Ocean, *J. Geophys. Res. Oceans*, *120*, 692–715, doi:10.1002/2014JC010139.

Hendon, H. H., C. Zhang, and J. D. Glick (1999), Interannual variation of the Madden-Julian Oscillation during austral summer, *J. Clim.*, *12*, 2538–2550.

Huffman, G. J., D. T. Bolvin, E. J. Nelkin, D. B. Wolff, R. F. Adler, G. Gu, Y. Hong, K. P. Bowman, and E. F. Stocker (2007), The TRMM multisatellite Precipitation Analysis (TMPA): Quasi-global, multiyear, combined-sensor precipitation estimates at fine scales, *J. Hydrometeorol.*, *8*, 38–55, doi:10.1175/JHM560.1.

Hung, M.-P., J.-L. Lin, W. Wang, D. Kim, T. Shinoda, and S. J. Weaver (2013), MJO and convectively coupled equatorial waves simulated by CMIP5 climate models, *J. Clim.*, *26*(17), 6185–6214.

Jayakumar, A., J. Vialard, M. Lengaigne, C. Gnanaseelan, J. P. McCreary, and B. Praveen Kumar (2011), Processes controlling the surface temperature signature of the Madden-Julian Oscillation in the thermocline ridge of the Indian Ocean, *Clim. Dyn.*, *37*, 2217–2234.

Jones, C., L. M. V. Carvalho, R. W. Higgins, D. E. Waliser, and J.-K. E. Schemm (2004), Climatology of tropical intraseasonal convective anomalies: 1979–2002, *J. Clim.*, *17*, 523–539.

Kessler, W. S., and R. Kleeman (2000), Rectification of the Madden-Julian oscillation into the ENSO cycle, *J. Clim.*, *13*, 3560–3575.

Kessler, W. S., M. J. McPhaden, and K. M. Weickmann (1995), Forcing of intraseasonal Kelvin waves in the equatorial Pacific, *J. Geophys. Res.*, *100*, 10,613–10,631, doi:10.1029/95JC00382.

Kirtman, B. P., and P. S. Schopf (1998), Decadal variability in ENSO predictability and prediction, *J. Clim.*, *11*, 2804–2822.

Kirtman, B. P., et al. (2014), The North American multimodel ensemble: Phase-1 seasonal-to-interannual prediction; Phase-2 toward developing intraseasonal prediction, *Bull. Am. Meteorol. Soc.*, *95*, 585–601, doi:10.1175/BAMS-D-12-00050.1.

Klingaman, N. P., X. Jiang, P. K. Xavier, J. Petch, D. Waliser, and S. J. Woolnough (2015), Vertical structure and physical processes of the Madden-Julian Oscillation: Synthesis and summary, *J. Geophys. Res. Atmos.*, *120*, 4671–4689, doi:10.1002/2015JD023196.

Kug, J.-S., F.-F. Jin, K. P. Sooraj, and I.-S. Kang (2008), State-dependent atmospheric noise associated with ENSO, *Geophys. Res. Lett.*, *35*, L05701, doi:10.1029/2007GL032017.

Lopez, H., and B. P. Kirtman (2013), Westerly wind bursts and the diversity of ENSO in CCSM3 and CCSM4, *Geophys. Res. Lett.*, *40*, 4722–4727, doi:10.1002/grl.50913.

Madden, R. A., and P. R. Julian (1972), Description of global-scale circulation cells in the tropics with a 40–50 day period, *J. Atmos. Sci.*, *29*, 1109–1123.

Madden, R. A., and P. R. Julian (1994), Observations of the 40–50-day tropical oscillation: A review, *Mon. Weather Rev.*, *122*, 814–837.

Maloney, E., and A. Sobel (2004), Surface fluxes and ocean coupling in the tropical intraseasonal oscillation, *J. Clim.*, *17*, 4368–4386.

Matthews, A. J., D. B. Baranowski, K. J. Keywood, P. J. Flatau, and S. Schimdtko (2014), The surface diurnal warm layer in the Indian Ocean during CINDY/DYNAMO, *J. Clim.*, *27*, 9101–9122.

McPhaden, M. J. (1999), Genesis and evolution of the 1997-98 El Niño, *Science*, *283*, 950–954.

Meehl, G. A., J. M. Arblaster, J. Caron, H. Annamalai, M. Jochum, A. Chakraborty, and R. Murtugudde (2012), Monsoon regimes and processes in CCSM4. Part 1: The Asian-Australian monsoon, *J. Clim.*, *25*, 2583–2608, doi:10.1175/JCLI-D-11-00184.1.

Moum, J. N., et al. (2014), Air-sea interactions from westerly wind bursts during the November 2011 MJO in the Indian Ocean, *Bull. Am. Meteorol. Soc.*, *95*(8), 1185–1199, doi:10.1175/BAMS-D-12-00225.1.

Neale, R. B., et al. (2010), Description of the NCAR Community Atmosphere Model (CAM 4.0), NCAR/TN-486+STR, NCAR, Boulder, Colo. [Available at http://www.cesm.ucar.edu/models/ccsm4.0/cam/docs/description/cam4_desc.pdf.]

Pohl, B., and A. J. Matthews (2007), Observed changes in the lifetime and amplitude of the Madden-Julian oscillation associated with interannual ENSO sea surface temperature anomalies, *J. Clim.*, *20*, 2659–2674.

Reynolds, R. W., T. M. Smith, C. Liu, D. B. Chelton, K. S. Casey, and M. G. Schlax (2007), Daily high-resolution-blended analyses for sea surface temperature, *J. Clim.*, *20*, 5473–5496, doi:10.1175/2007JCLI1824.1.

Saji, N. H., B. N. Goswami, P. N. Vinayachandran, and T. Yamagata (1999), A dipole mode in the tropical Indian Ocean, *Nature*, *401*(6751), 360–363.

Slingo, J. M., D. P. Rowell, K. R. Sperber, and F. Nortley (1999), On the predictability of the interannual behaviour of the Madden-Julian Oscillation and its relationship with el Niño, *Q. J. R. Meteorol. Soc.*, *125*, 583–609, doi:10.1002/qj.49712555411.

Sobel, A. H., and E. D. Maloney (2013), Moisture modes and the eastward propagation of the MJO, *J. Atmos. Sci.*, *70*, 187–192.

Tam, C.-Y., and N.-C. Lau (2005), Modulation of the Madden-Julian Oscillation by ENSO: Inferences from observations and GCM simulations, *J. Meteorol. Soc. Jpn.*, *83*, 727–743.

Vialard, J., et al. (2009), Cirene: Air-sea interactions in the Seychelles-Chagos Thermocline Ridge region, *Bull. Am. Meteorol. Soc.*, *90*, 45–61, doi:10.1175/2008BAMS2499.2.

Waliser, D. E., K. M. Lau, and J.-H. Kim (1999), The Influence of Coupled Sea Surface Temperatures on the Madden-Julian Oscillation: A Model Perturbation Experiment, *J. Atmos. Sci.*, *56*, 333–358.

Waliser, D. E., K. M. Lau, W. Stern, and C. Jones (2003), Potential predictability of the Madden-Julian Oscillation, *Bull. Am. Meteorol. Soc.*, *84*(1), 33–50.

Webster, P. J., A. M. Moore, J. P. Loschnigg, and R. R. Leben (1999), The great Indian Ocean warming of 1997–98: Evidence of coupled oceanic-atmospheric instabilities, *Nature*, *401*, 356–360.

Weickmann, K. M. (1991), El Niño/Southern Oscillation and Madden-Julian (30–60 day) oscillations during 1981–1982, *J. Geophys. Res.*, *96*, 3187–3195, doi:10.1029/90JD01832.

Woolnough, S., J. Slingo, and B. Hoskins (2000), The relationship between convection and sea surface temperature on intraseasonal timescales, *J. Clim.*, *13*, 2086–2104.

Xie, S.-P., H. Annamalai, F. A. Schott, and J. P. McCreary Jr. (2002), Structure and mechanisms of south Indian Ocean climate variability, *J. Clim.*, *15*, 864–878.

Yu, L., X. Jin, and R. A. Weller (2008), Multidecade global flux datasets from the Objectively Analyzed Air-sea Fluxes (OAFlux) Project: Latent and sensible heat fluxes, ocean evaporation, and related surface meteorological variables, Woods Hole Oceanographic Institution, OAFlux Project Tech. Rep., OA-2008-01, pp. 1–64, Woods Hole, Mass.

Zhang, C. (2013), Madden-Julian Oscillation: Bridging weather and climate, *Bull. Am. Meteorol. Soc.*, *94*, 1849–1870, doi:10.1175/BAMS-D-12-00026.1.